International Journal of Mass Spectrometry 453 (2020) 116354

Contents lists available at ScienceDirect

International Journal of Mass Spectrometry

journal homepage: www.elsevier.com/locate/ijms

Fragmentation pathways of odd- and even-electron *N*-alkylated synthetic cathinones

J. Tyler Davidson, PhD [a], Zachary J. Sasiene, BS [b], Glen P. Jackson, Ph.D. [a, b, *]

[a] Department of Forensic and Investigative Science, West Virginia University, Morgantown, WV, 26506-6121, USA
[b] C. Eugene Bennett Department of Chemistry, West Virginia University, Morgantown, WV, 26506-6121, USA

ARTICLE INFO

Article history:
Received 19 March 2020
Received in revised form
17 April 2020
Accepted 18 April 2020
Available online 23 April 2020

ABSTRACT

Three ionization techniques, isotopic labeling, high-resolution mass spectrometry (HRMS) and multi-stage mass spectrometry (MS^n) were used to analyze a series of *N*-alkylated synthetic cathinone derivatives and gain a deeper understanding of their fragmentation behavior during mass spectrometric analysis. The compounds analyzed represent 15 unique structures with common substitutions to the core synthetic cathinone structure, including substitutions to the aromatic ring and the number and types of *N*-alkyl functionalities. The analytical techniques employed include gas chromatography-electron ionization-mass spectrometry (GC-EI-MS), electrospray ionization-tandem mass spectrometry (ESI-MS/MS) with HRMS and direct analysis in real time tandem mass spectrometry (DART-MS/MS) with HRMS. These techniques cover a variety of forensic applications, including seized drug analysis, toxicological analysis and screening analysis, in local, state and federal laboratories. For collision-induced dissociation (CID) of protonated precursors, the spectra of 2° and 3° amines showed evidence for charge-remote and charge-directed fragmentation mechanisms. The 2° amines lost H_2O as a dominant pathway whereas the 3° amines favored the formation of alkylphenones. As reported by others, CID of protonated *N*-alkylated cathinones containing 2° and 3°amines also provided an abundance of odd-electron product ions from the even-electron precursors. In contrast to the rearrangements observed in CID of protonated cathinones, EI fragmentation patterns were dominated by radical-directed cleavages to form iminium ions and charge-directed cleavages to form acylium ions. A comparison between the fragmentation behaviors of *N*-alkylated synthetic cathinones under all three ionization techniques enables a deeper understanding of *N*-alkylated synthetic cathinone fragmentation under varying instrumental setups.

1. Introduction

N-alkylated synthetic cathinones are analogs of the natural product cathinone, which is derived from the leaves of the *Catha edulis* plant, commonly referred to as khat. Khat is a native plant to the Horn of Africa and the Southwest Arabian Peninsula that, when chewed, produces stimulant-like effects [1,2]. The stimulant properties of cathinones are typically stronger than over-the-counter stimulants like caffeine and nicotine, and similar to the effects of amphetamines, which are structurally similar to cathinones [3]. *N*-alkylated synthetic cathinones are characterized by alkyl side chains on the amine moiety of the generic benzoylethanamine structure. Additional analogs within this class include those with aliphatic substitutions to the alkyl chain and with substitutions to the benzene ring. The *N*-alkylated class of cathinones was the first class of synthetic cathinone derivatives to become available on the drug market [1].

In the 1930s, methcathinone was marketed under the name ephedrone as an antidepressant in the USSR. Methcathinone was also developed as a central nervous system stimulant by the Parke Davis pharmaceutical company in the United States [3]. In the 1950s, the *N*-alkylated synthetic cathinone diethylpropion was marketed under the name amfepramone as an appetite suppressant [4]. Whereas *N*-alkylated synthetic cathinones were originally developed for therapeutic purposes, the 1970s brought reports of methcathinone abuse in the Soviet Union. By the 1990s, the United States also documented methcathinone abuse [5]. Due to the low cost and psychostimulant nature of synthetic

* Corresponding author. Department of Forensic and Investigative Science, West Virginia University, Morgantown, WV, 26506-6121, USA.
E-mail addresses: jtdavidson@mix.wvu.edu (J.T. Davidson), zjs0005@mix.wvu.edu (Z.J. Sasiene), glen.jackson@mail.wvu.edu (G.P. Jackson).

https://doi.org/10.1016/j.ijms.2020.116354
1387-3806/

cathinones, substances such as 3,4-methylenedioxymethcathinone, better known as methylone were sold in head shops and the internet by the early 2000s [6]. The main reason for abuse of synthetic cathinones was for their recreational use at dance clubs and parties [1].

Currently, synthetic cathinones are marketed as "not for human consumption" or "bath salts" to avoid legislative restrictions imposed to decrease the sale and distribution of these compounds [7,8]. The reported symptoms of synthetic cathinone abuse include euphoria, hallucinations, psychosis, paranoia, agitation, violent behavior, tachycardia, acidosis, seizures, and even death [9,10]. The first *N*-alkylated synthetic cathinone to be classified as a schedule I substance by the Drug Enforcement Administration (DEA) was methcathinone in 1993 [11], but the rapid modifications to the generic synthetic cathinone structure make it difficult to regulate. The clandestine synthesis of analogs with only minor modifications to the generic structure provides a way around the imposed regulations while also introducing potentially more harmful substances onto the illicit drug market [1,12].

This project describes the fragmentation pathways of *N*-alkylated synthetic cathinones using three common analytical techniques available to crime laboratories and national laboratories, including GC-EI-MS, ESI-MS/MS, and DART-HRMS. The DART source was mounted on a quadrupole time-of-flight (Q-TOF) mass spectrometer, which also enables high-resolution MS/MS acquisition. These setups are representative of the instrumentation commonly employed in seized drug laboratories, toxicological laboratories, and national laboratories, respectively. The comparison of the fragmentation mechanisms of odd-electron ions (EI) and even-electron ions (ESI) provides a more comprehensive understanding of the differences in fragmentation behavior.

The fragmentation behavior of *N*-alkylated synthetic cathinones has been reported throughout literature; however, the underlying fragmentation mechanisms that lead to the observed fragment ions are rarely discussed or understood [13–16]. Examples of the confusion about the formation of the tropylium ion from protonated synthetic cathinones have been highlighted previously by our group [17]. Even when mechanisms have been proposed, the lack of isotopic labeling and multi-stage mass spectrometry limits the certainty associated with the proposed mechanisms [18]. Specific examples of reported *N*-alkylated fragmentation behavior without mechanistic understanding including the works of Jankovics et al. [19], Martinez-Clemente et al. [20], and Fornal [21]. These articles provide useful fragmentation pathways but highlight that the mechanistic explanation for the fragmentation behavior of *N*-alkylated synthetic cathinones remain unclear. By gaining a better understanding of the fragmentation mechanisms, analysts would be better positioned to both defend the data of known scheduled drugs and to perform structural characterization to identify novel psychoactive substances (NPS) entering the market [16].

The goal of this project is to better understand the fragmentation pathways of *N*-alkylated synthetic cathinones. The developed fragmentation pathways and mechanistic explanations will help advance the current understanding of the behavior of *N*-alkylated synthetic cathinones under different ionization and fragmentation conditions. Specifically, the comparison between the fragmentation behavior of odd-electron (via EI) and even-electron (via ESI and DART) ions of different *N*-alkylated synthetic cathinones provides a more comprehensive understanding of these compounds. This project combines isotopic labeling, MS^n, and accurate mass measurements with HRMS to confirm the mechanisms of odd-electron and even-electron fragmentation of *N*-alkylated synthetic cathinones.

2. Methods

2.1. Sample preparation

The ten standards purchased through Cayman Chemical (Ann Arbor, MI, USA) were methcathinone, ethcathinone, pentedrone, buphedrone, α-propylaminopentiophenone, *N*-ethylbuphedrone, 3,4-dimethyl-α-ethylaminovalerophenone, methylone, butylone, and pentylone. The nine standards purchased through Cerilliant (Round Rock, TX, USA) were methcathinone-d_3 (*N*-alkyl deuterated), diethylpropion, diethylpropion-d_{10} (*N*-alkyl deuterated), ^{13}C-benzedrone (^{13}C on carbonyl carbon), ^{13}C-ethylone (^{13}C on carbonyl carbon), ^{13}C-butylone (^{13}C on carbonyl carbon), pentylone-d_3 (*N*-alkyl deuterated), dibutylone-d_3 (alkyl deuterated), and eutylone-d_5 (*N*-alkyl deuterated). The non-deuterated samples were prepared in a solution of 49% HPLC grade methanol, 49% distilled water, and 2% acetic acid. The HPLC grade methanol was supplied by Fisher Scientific (Palo Alto, CA) and the acetic acid was supplied by Acros Organics (Palo Alto, CA). The deuterated samples were left in the original methanol solvent. All samples were prepared to a final concentration of approximately 100 ppm.

2.2. Instrumentation

2.2.1. Linear ion trap

A Thermo Scientific Velos Pro linear ion trap (LIT) mass spectrometer was operated with a heated-electrospray ionization (HESI) source at 50 °C. The spray voltage was 4,000 V with the nitrogen sheath gas flow set to 8 arbitrary units and the nitrogen auxiliary flow set to 5 arbitrary units. The mass spectrometer capillary temperature was set to 275 °C. The scan range and normalized collision energy (NCE) were specific for each compound and are labeled with each mass spectrum. The bath gas was ultra-pure helium from Matheson TRIGAS (Fairmont, WV, USA).

2.2.2. Quadrupole time-of-flight

An Agilent Technologies 6538 UHD Accurate-Mass Quadrupole Time-of-flight (Q-TOF) mass spectrometer was operated with both a dual ESI source and a DART source. The DART-100 source was mounted to the Q-TOF with a Vapur® interface (IonSense, Saugus, MA, USA). The DART ion source was operated with helium gas at 300 °C, with a flow rate of 3.0 L/min, a grid voltage of 400 V and a needle voltage of 3,500 V. The ESI source was operated with a spray voltage of 3,500 V, with a 300 °C nitrogen drying gas flow rate of 5 L/min and a nebulizer flow of 30 psig. The MS fragmentor and skimmer voltages, the scan range and collision energy were specific for each compound and are labeled with each mass spectrum. An isolation width of 1.3 Da was used for all samples. The ultra-high purity nitrogen and helium used for the collision gas and DART gas, respectively, were from Matheson TRIGAS (Fairmont, WV, USA).

The DART samples were prepared through the deposition of 5 μL of drug standard onto the closed end of a 1.5 × 1.8 × 90 mm Pyrex® glass capillary purchased through Corning Life Sciences (Corning, New York, USA). Once the samples were dry, the DART analysis consisted of approximately 30 s of background collection, about 5 s of sample introduction, and then the analysis of a blank capillary to account for capillary specific background. The total length of analysis was less than 90 s per sample.

2.2.3. Single quadrupole GC-EI-MS

An Agilent Technologies 7890 GC-5977 MS with a HP-5 ((5% phenyl)-methylpolysiloxane) 30 m × 250 μm × 0.25 μm column manufactured by Agilent J&W Columns was used for these analyses. The GC-EI-MS parameters were as follows: injection volume

was 1 μL; injection temperature was 250 °C; split ratio was 20:1. The initial oven temperature was 80 °C (1 min hold), which was ramped to 280 °C at 15 °C/min, then held for 2 min. The carrier gas (helium) flow rate was set to 1 mL/min and the transfer line temperature was set to 280 °C. The ultra-high purity helium gas was purchased through Matheson TRIGAS (Fairmont, WV, USA). The mass spectrometer was scanned from *m/z* 50−500 after a solvent delay of 2 min. The scan rate was 1,500 Da/sec. The source and quadrupole temperatures were 250 °C and 200 °C, respectively.

2.3. Data analysis

Xcalibur 2.0.0.48 software was used for the data analysis on the Velos Pro instrument. MassHunter Qualitative Analysis B.05.00 was used for the Agilent Q-TOF data analysis, and ChemStation version C.01.01 was used for the Agilent GC-EI-MS data analysis. Microsoft Excel version 14 (Microsoft, Redmond, WA, USA) and ChemDraw 16.0 (PerkinElmer, Waltham, MA, USA) were used for mass spectral plots and mass spectral fragmentation mechanisms.

2.3.1. Mass spectral interpretation and mechanisms

The mass spectral fragmentation mechanisms proposed are based on the combination of isotopic labeling, MS^n and accurate mass measurements with HRMS. The mechanisms follow the expected lowest energy pathways [22], which often involve charge-remote 4- or 6-center eliminations consistent with the previous literature [23,24]. The isotopic labeling consisted of perdeuteration on both the aliphatic chain and the *N*-alkyl chains and ^{13}C on the carbonyl carbons. These isotopic labels provide useful isotopic shifts relative to unlabeled compounds. Even though it is not always possible to know the exact location of the hydrogen atoms or deuterium atoms in certain rearrangements, the use of HRMS and MS^n helps identify the elemental composition and information about the structure of intermediates along the proposed pathways, respectively. In the present work, the *N*-alkylated class of synthetic cathinones frequently form odd-electron product ions from even-electron (e.g. protonated) precursor ions, which is consistent with prior work [13,25].

3. Results and discussion

3.1. HESI-Velos Pro MS^n

Fig. 1 shows the MS^n fragmentation of pentedrone with the major structural fragments embedded. Isolation and fragmentation of the protonated precursor ion $[M+H]^+$ at *m/z* 192 results in the production of two dominant product ions at *m/z* 174 and *m/z* 161 (Fig. 1a). The product ion at *m/z* 174 forms through the loss of H_2O, whereas the product ion at *m/z* 161 forms through the loss of the *N*-alkylated moiety. Fig. 1b shows the MS^3 spectrum from the isolation and fragmentation of the primary product ion at *m/z* 174. The major secondary fragments of *m/z* 174 appear at *m/z* 159, 145, 132, and 131. These losses are consistent with the loss of a methyl radical ($^{\cdot}CH_3$), ethyl radical ($^{\cdot}C_2H_5$), propene (C_3H_6) and propyl radical ($^{\cdot}C_3H_7$), respectively, with the propene pathway being the most abundant pathway. Fig. 1c shows the resulting spectrum from the isolation and fragmentation of the primary product ion at *m/z* 161. The secondary product ions observed from the primary fragment at *m/z* 161 are consistent with the valerophenone ion fragmentation pathways previously demonstrated by our group [26] including the dominant tropylium ion. As described previously for α-pyrrolidinophenone synthetic cathinones, the tropylium ion almost certainly contains the α-carbon and not the carbonyl carbon and forms via phthalane-like intermediates at *m/z* 119 and *m/z* 133 [17].

Fig. 2 contains the MS^n fragmentation of pentylone with the major structural fragments embedded. Pentylone is the methylenedioxy substituted equivalent of pentedrone and has a protonated precursor ion at *m/z* 236, which is 44 Da larger than pentedrone. The product ion spectrum of pentylone obtained on the LIT shows product ions at *m/z* 218, 205, 188, 175, and 86. The primary product ions at *m/z* 218 and *m/z* 205 are consistent with the methylenedioxy derivatives of the primary product ions observed for pentedrone at *m/z* 174 and *m/z* 161, respectively. Also, the methylenedioxy substitution provides two additional fragmentation pathways not available or prominent for pentedrone; they are the loss of formaldehyde (CH_2O, 30 Da) from the substituted valerophenone-like intermediate and the formation of an iminium ion, as seen by the product ions at *m/z* 175 and *m/z* 86, respectively.

Fig. 2b shows the MS^3 spectrum following isolation and fragmentation of the primary product ion at *m/z* 218, which results in the formation of secondary product ions at *m/z* 188, 176, and 175. The secondary product ions are consistent with the loss of formaldehyde (CH_2O), propene (C_3H_6), and a propyl radical ($^{\cdot}C_3H_7$) from the vinyl intermediate at *m/z* 218, with the loss of formaldehyde from the methylenedioxy group being the most abundant pathway. Fig. 2c shows the resulting mass spectrum from the isolation and fragmentation of the primary product ion at *m/z* 205, which again is dominated by the loss of formaldehyde at *m/z* 175 and the formation of the methylenedioxy-substituted tropylium ion at *m/z* 135 [17].

Fig. 3a shows the tandem mass spectrum of dibutylone-d_3, which is deuterated on the end of the aliphatic chain. The major structural fragments are embedded. Isolation and fragmentation of the protonated precursor ion $[M+H]^+$ at *m/z* 239 results in the formation of major product ions at *m/z* 194, 149, and 89. The primary product ion at *m/z* 194 forms through the loss of the *N*-alkylated moiety whereas the product ions at *m/z* 149 and *m/z* 89 are the methylenedioxy substituted benzoylium ion and a deuterated iminium ion, respectively. The significance of the tandem mass spectrum in Fig. 3a is that, in contrast to pentedrone in Fig. 1a, the loss of H_2O from dibutylone-d_3 is negligible. We presume that the *N,N*-demethylation hinders hydrogen transfer to the carbonyl oxygen and makes a more labile leaving group, both of which make the loss of the *N*-alkylated moiety the base peak for dibutylone-d_3. Of the 15 unique *N*-alkylated structures studied, the only other compound to lose the *N*-alkylated moiety in preference to H_2O was diethylpropion, which is also a 3° amine.

Isolation and fragmentation of the primary product ion of dibutylone-d_3 at *m/z* 194 results in the formation of secondary product ions at *m/z* 166 and *m/z* 164, which form through the neutral losses of CO and formaldehyde (CH_2O), respectively (Fig. 3b). Based on MS^n analysis (not shown), the tertiary product ion at *m/z* 136 forms through the loss of CO from the intermediate product ion at *m/z* 164 and the loss of formaldehyde from the intermediate at *m/z* 166. Fig. 3c shows the MS^3 mass spectrum that results from the isolation and fragmentation of the primary product ion at *m/z* 89. Interestingly, Fig. 3c shows the presence of product ions at both *m/z* 74 and *m/z* 71 for the losses of $^{\cdot}CH_3$ or $^{\cdot}CD_3$ radicals, respectively, with a clear preference to lose the terminal $^{\cdot}CD_3$ group most distal to the nitrogen.

3.2. DART/ESI-Q-TOF

Fig. 4 compares ESI and DART MS/MS spectra of methcathinone-d_3 with the major structural fragments embedded. The fragment ion *m/z* values and abundances for DART-MS/MS and ESI-MS/MS are generally similar throughout the spectra. One notable difference between the DART- and ESI-generated mass spectra is the presence of $[M+H]^+$ precursor ion at *m/z* 167.1322 ($C_{10}H_{11}D_3NO^+$

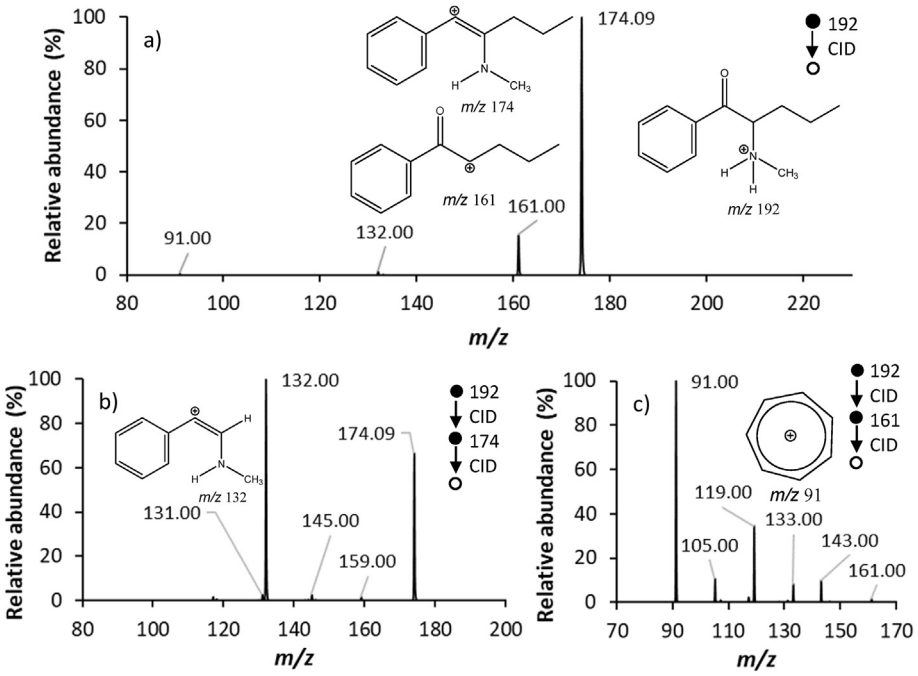

Fig. 1. Product ion mass spectra of pentedrone on the LIT: a) MS^2 product ion spectrum of the $[M+H]^+$ molecular ion (30% NCE); b) MS^3 product ion spectrum of the product ion at *m/z* 174 (30% NCE) showing the formation of secondary product ions at *m/z* 159, 145, 132, and 131; c) MS^3 product ion spectrum of the primary product ion at *m/z* 161 (30% NCE) showing the characteristic valerophenone ion fragmentation.

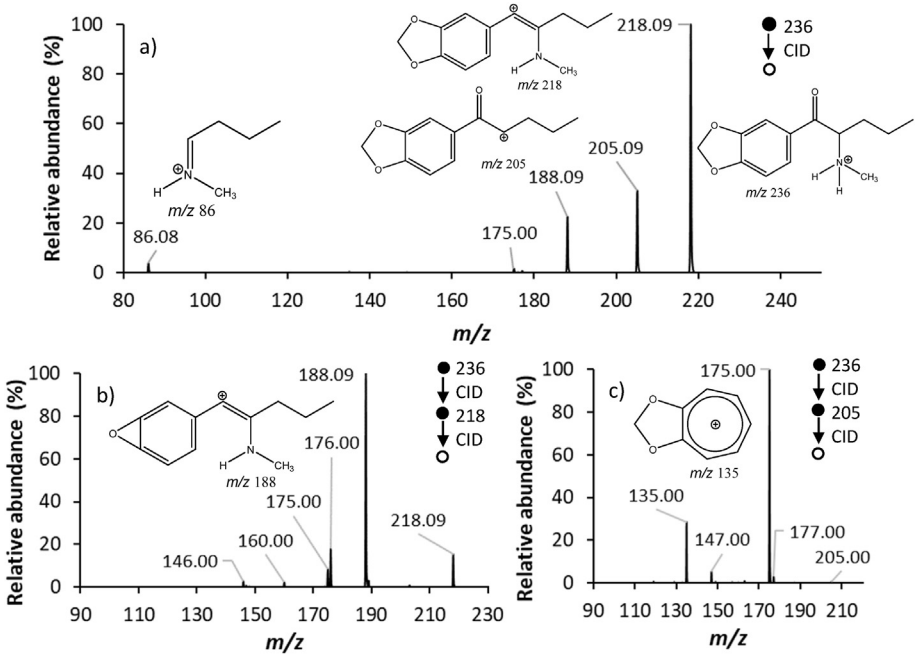

Fig. 2. Product ion mass spectra of pentylone: a) MS^2 product ion spectrum of the $[M+H]^+$ molecular ion (30% NCE); b) MS^3 product ion spectrum of the product ion at *m/z* 218 (30% NCE) showing the formation of secondary product ions at *m/z* 188, 176, 175, 160, and 146; c) MS^3 product ion spectrum of the primary product ion at *m/z* 205 (30% NCE) showing the characteristic methylenedioxy valerophenone ion fragmentation.

expected at *m/z* 167.1260; 37 ppm error) in the DART mass spectra. The collision energy was kept constant at 25 eV for both ion sources, but ESI had an additional 25 V on the fragmentor voltage setting to assist the in-source declustering of ions from the ion source. Apparently, the additional 25 V fragmentor potential for ESI imparts more internal energy to the ions and causes them to enter the collision cell with an elevated internal energy relative to the same ions entering from the DART source.

The main structural fragments of interest are observed in the ESI-generated product ion spectrum at *m/z* 149.1160 ($C_{10}H_9D_3N^+$ expected at *m/z* 149.1154; 6 ppm error), *m/z* 134.0960 ($C_9H_6D_3N^+$ expected at *m/z* 134.0920; 30 ppm error), 133.0730 ($C_9H_9O^+$ expected at *m/z* 133.0653; 58 ppm error), and *m/z* 131.0744 ($C_9H_9N^+$ expected at *m/z* 131.0734; 8 ppm error), which are formed through

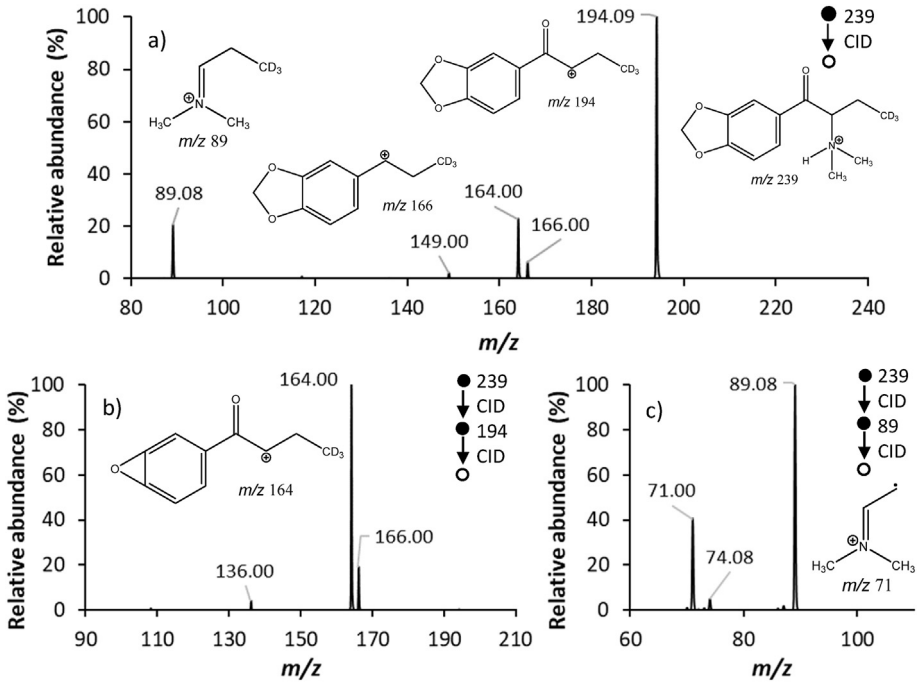

Fig. 3. Product ion mass spectra of dibutylone-d_3 on the LIT: a) MS^2 product ion spectrum of the $[M+H]^+$ molecular ion (30% NCE); b) MS^3 product ion spectrum of the primary product ion at *m/z* 194 (30% NCE) showing the formation of product ions at *m/z* 166, 164, and 136; c) MS^3 product ion spectrum of the primary product ion at *m/z* 89 (30% NCE) showing the loss of both a methyl radical and a deuterated methyl radical.

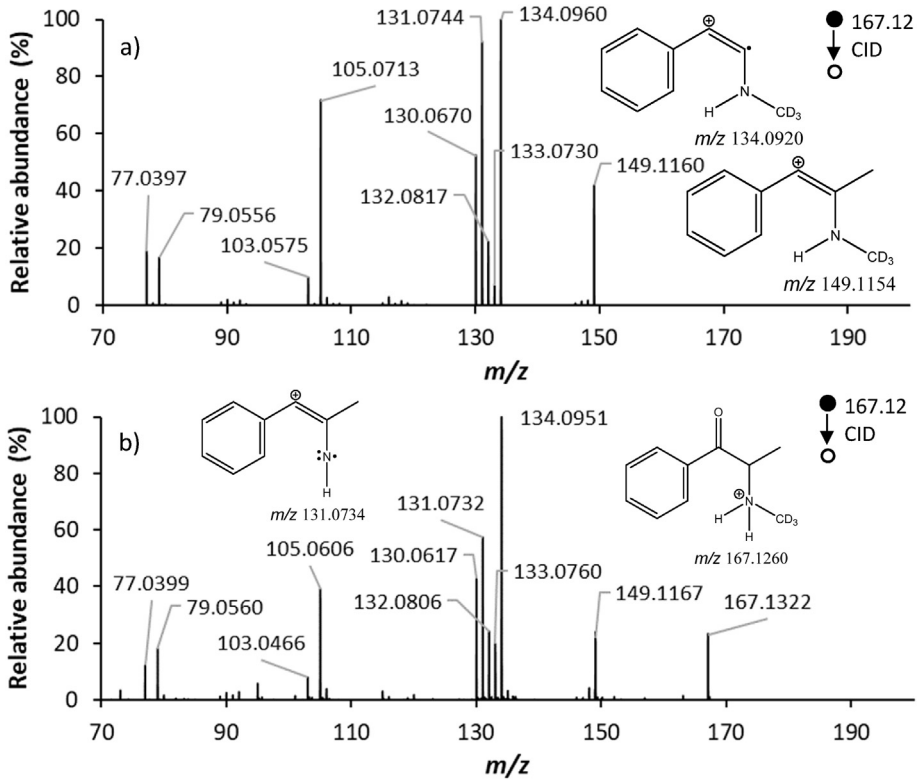

Fig. 4. Tandem mass spectra of methcathinone-d_3 collected on the Q-TOF with both a) ESI and b) DART ionization with a collision energy of 25 eV and skimmer voltage of 65 V. The ESI spectrum was collected with a fragmentor voltage of 175 V, whereas the DART spectrum was collected with a fragmentor voltage of 150 V.

the loss of H_2O, a methyl radical ($^{\bullet}CH_3$), the *N*-alkylated moiety and a deuterated methyl radical ($^{\bullet}CD_3$), respectively. The high-resolution of the Q-TOF instrument permits the determination of elemental formulas for diagnostic ions through their measured accurate masses. The accurate mass measurements of the product ions at *m/z* 149.1160 ($C_{10}H_9D_3N^+$) and *m/z* 131.0744 ($^{\bullet}C_9H_9N^+$) are less than 10 ppm from the exact masses for the proposed structures, whereas the accurate mass measurements for the product ions at *m/z*

134.0960 ($\dot{C}_9H_6D_3N^+$) and *m/z* 133.0730 ($C_9H_9O^+$) were approximately 3–5 times further from the exact masses for the proposed structures. Even with the expanded error, these sub-60 ppm differences between measured accurate masses and theoretical exact masses provides sufficient confidence to rely on the proposed elemental compositions. Likewise, the mass-dependence of ppm values inflates these reported errors relative to larger molecular weight compounds. If the mass errors discussed above were reported in mDa, as suggested by others [27], our values range from less than 1 mDa to 8 mDa.

Based on the MS^n analysis on the LIT, the product ions in the ESI-generated product ion spectrum at *m/z* 105.0713 ($C_8H_9^+$ expected at *m/z* 105.0704; 9 ppm error), *m/z* 103.0575 ($C_8H_7^+$ expected at *m/z* 103.0547; 27 ppm error), *m/z* 79.0556 ($C_6H_7^+$ expected at *m/z* 79.0547; 11 ppm error), and *m/z* 77.0397 ($C_6H_5^+$ expected at *m/z* 77.0391; 8 ppm error) originate from the intermediate product ion at *m/z* 133.0730 ($C_9H_9O^+$), whereas the product ions at *m/z* 132.0817 ($C_9H_6D_2N^+$ expected at *m/z* 132.0780; 28 ppm error) and *m/z* 130.0670 ($C_9H_8N^+$ expected at *m/z* 130.0656; 11 ppm error) originate from the intermediate product ions at *m/z* 134.0960 ($\dot{C}_9H_6D_3N^+$) and *m/z* 131.0744 ($\dot{C}_9H_9N^+$), respectively. Of all the cathinones studied, the only notable differences between MS/MS data from the DART and ESI ion sources were the abundances of the precursor ion; some residual precursor was always observed for the DART-generated precursors. Likewise, small, but insignificant, differences in the accurate mass measurements were observed between the ESI- and DART-generated mass spectra due to random variance in arrival times of the ions. If needed, the mass accuracy could be improved by the inclusion of internal mass calibrants. However, the internal calibration solution is known to provide several low-mass fragments, such as *m/z* 121 and *m/z* 149, which are also expected in methylenedioxy-containing synthetic cathinones. To prevent possible interference, we deactivated the internal mass calibration in these studies.

The comparison between the ESI- and DART-generated mass spectra for diethylpropion-d_{10} (perdeuterated on the diethylpropion moiety) in Fig. 5 provides further support for the similarity between ESI and DART mass spectra. The accurate mass of the ESI-generated mass spectrum at *m/z* 105.0713 is closer to the exact mass for $C_8H_9^+$ at *m/z* 105.0704 (9 ppm error) rather than for $C_7H_5O^+$ at *m/z* 105.0340 (355 ppm error; 37 mDa). The accurate mass data indicates the primary product ion at *m/z* 133.0690 ($C_9H_9O^+$ expected at *m/z* 133.0653; 28 ppm error) loses CO instead of C_2H_4 to yield *m/z* 105.0713 ($C_8H_9^+$). The product ion at *m/z* 110.1786 ($C_6H_4D_{10}N^+$ expected at *m/z* 110.1743; 39 ppm error) is the iminium-d_{10} ion, whereas the product ion at *m/z* 84.1616 ($C_4H_2D_{10}N^+$ expected at *m/z* 84.1587; 38 ppm error) is the diethylamine-d_{10} ion. As mentioned earlier, diethylpropion-d_{10} is one of the two 3° amines analyzed during this study, and the elevated abundance of the product ion at *m/z* 105.0713 ($C_8H_9^+$) shows that the loss of the *N*-alkylated moiety is favored over the loss of H_2O for 3° amines. This hypothesis is supported by previous research highlighting the dominant pathway through the loss of H_2O and secondary fragmentation for 2° amine synthetic cathinones [25].

Fig. 6 is a comparison between the ESI and DART spectra of protonated eutylone-d_5 $[M+H]^+$ at *m/z* 241.15 with the major structural fragments embedded. The ESI-generated product ion spectrum shows the presence of primary product ions at *m/z* 223.1516 ($C_{13}H_{11}D_5O_2N^+$ expected at *m/z* 223.1489; 12 ppm error), *m/z* 191.0738 ($C_{11}H_{11}O_3^+$ expected at *m/z* 191.0708; 16 ppm error), *m/z* 149.0262 ($C_8H_5O_3^+$ expected at *m/z* 149.0238; 16 ppm error) and *m/z* 91.1324 ($C_5H_7D_5N^+$ expected at *m/z* 91.1278; 51 ppm error) as well as secondary product ions at *m/z* 194.1161 ($\dot{C}_{11}H_6D_5O_2N^+$ expected at *m/z* 194.1098; 32 ppm error), *m/z* 193.1442 ($C_{12}H_9D_5ON^+$ expected at *m/z* 193.1384; 30 ppm error) and *m/z* 161.0666 ($C_{10}H_9O_2^+$ expected at *m/z* 161.0602; 40 ppm error). The tertiary product ions at 135.0479 ($C_8H_7O_2^+$ expected at *m/z* 135.0446; 24 ppm error) and 133.0701 ($C_9H_9O^+$ expected at *m/z* 133.0653; 36 ppm error) originate from the secondary product ion at 191.0738 ($C_{11}H_{11}O_3^+$). The primary product ions at *m/z* 223.1516 ($C_{13}H_{11}D_5O_2N^+$) and *m/z* 191.0738 ($C_{11}H_{11}O_3^+$) form through the loss of H_2O and the loss of the *N*-alkylated moiety, respectively, whereas the primary product ions at *m/z* 149.0262 ($C_8H_5O_3^+$) and *m/z* 91.1324 ($C_5H_7D_5N^+$) correspond to the methylenedioxy-substituted benzoylium ion and the imminium-d_5 ion, respectively. The secondary product ions at *m/z* 194.1161 ($\dot{C}_{11}H_7D_5O_2N^+$) and *m/z* 193.1442 ($C_{12}H_9D_5ON^+$) form, respectively, through the loss of an ethyl radical ($\dot{C}_2H_5$) and formaldehyde (CH_2O) from the intermediate ion at *m/z* 223.1516 ($C_{13}H_{11}D_5O_2N^+$), whereas the secondary product ion at *m/z* 161.0666 ($C_{10}H_9O_2^+$) forms through the loss of formaldehyde (CH_2O) from the intermediate ion at *m/z* 191.0738 ($C_{11}H_{11}O_3^+$). The error between the accurate mass measurements and the exact masses of the elemental compositions shown were the smallest errors of all possible elemental compositions and within approximately 50 ppm, which once again corresponds to <7 mDa error. The HRMS accuracy is sufficient to provide unambiguous elemental compositions and a reasonable indication of the proposed structures.

The supplemental material contains six additional figures of the LIT and Q-TOF data for the remaining compounds in this study. Fig. 7 shows the proposed fragmentation mechanisms for the *N*-alkylated class of synthetic cathinones, where X represents substitution to the phenyl moiety and C_nH_{2n+1} represents varying alkyl chain lengths. The ^{13}C and deuterium labels are not shown in the proposed fragmentation mechanisms, but standards containing these isotopic labels were used to support the proposed mechanisms.

The primary fragmentation pathways for the *N*-alkylated class of synthetic cathinones are through the loss of H_2O (blue pathway), $C_nH_{2n+3}N$ (black pathway), and C_7H_6O (red pathway), which is consistent with previous work by others on this class of compounds [13,18,19,28–30]. The dominant pathway for 2° amines within this class is through the loss of H_2O via two hydrogen transfers to the oxygen. Deuterium labeling on the *N*-alkyl group (e.g. methcathinone-d_3 in Fig. 4 and eutylone-d_5 in Fig. 6) showed that the hydrogens from the *N*-alkyl group do not contribute to the neutral loss of H_2O. Similarly, CID of dibutylone-d_3 (alkyl deuterated) provided evidence that the terminal hydrogens on the alkyl chain do not participate in the H_2O loss. Therefore, the hydrogens must originate from the charging proton and from hydrogen atoms nearer to the carbonyl group, as proposed in the 4-center elimination in Fig. 7.

Several structures have been proposed for the loss of H_2O from synthetic cathinones; however, the previous studies did not use isotopic labeling and HRMS [13,18,19,28–30]. Our data supports a mechanism similar to the one proposed in Fig. 7. Following the loss of H_2O, the intermediate at *m/z* 174 may then lose a methyl radical ($\dot{C}H_3$) from the *N*-alkyl group (green pathway), as supported by the loss of the deuterated methyl radical ($\dot{C}D_3$) from the methcathinone-d_3 intermediate at *m/z* 149.1160 (Fig. 4). In both cases the radical loss would be impossible if the double bond of the iminium intermediate was between the N atom and the *N*-alkylated moiety.

Secondary fragmentation also occurs through the loss of alkyl radicals from the aliphatic chain (gold pathway), alkyl radicals from the *N*-alkylated moiety (green pathways), and even-electron alkenes through 4- or 6-center eliminations along the aliphatic chain (blue pathways). The presence of distonic radicals (like the structures at *m/z* 131 and *m/z* 159), along with the loss of H_2O, was observed for every 2° amine *N*-alkylated synthetic cathinone analyzed in this study.

The second most abundant fragmentation pathway for 2° amine

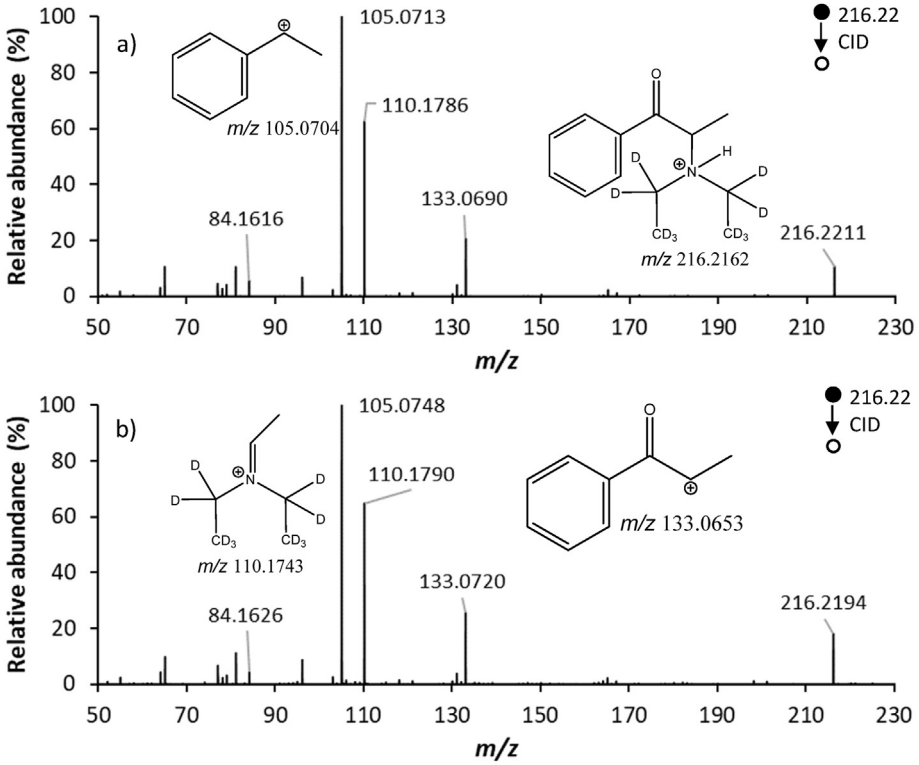

Fig. 5. Tandem mass spectra of diethylpropion-d_{10} collected on the Q-TOF with both a) ESI and b) DART ionization with a collision energy of 25 eV. The ESI spectrum was collected with a fragmentor voltage of 225 V, whereas the DART spectrum was collected with a fragmentor voltage of 150 V, which were both collected with a skimmer voltage of 65 V.

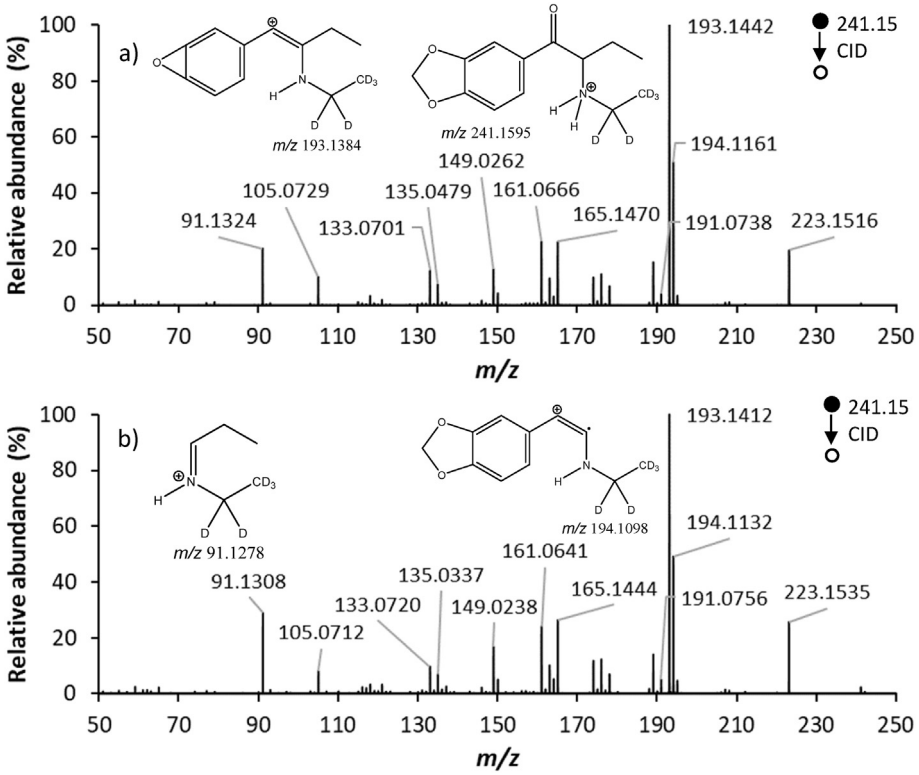

Fig. 6. Tandem mass spectra of eutylone-d_5 collected with both a) ESI and b) DART ionization with a collision energy of 25 eV. The ESI spectrum was collected with a fragmentor voltage of 225 V whereas the DART spectrum was collected with a fragmentor voltage of 150 V. Both were collected with a skimmer voltage of 65 V.

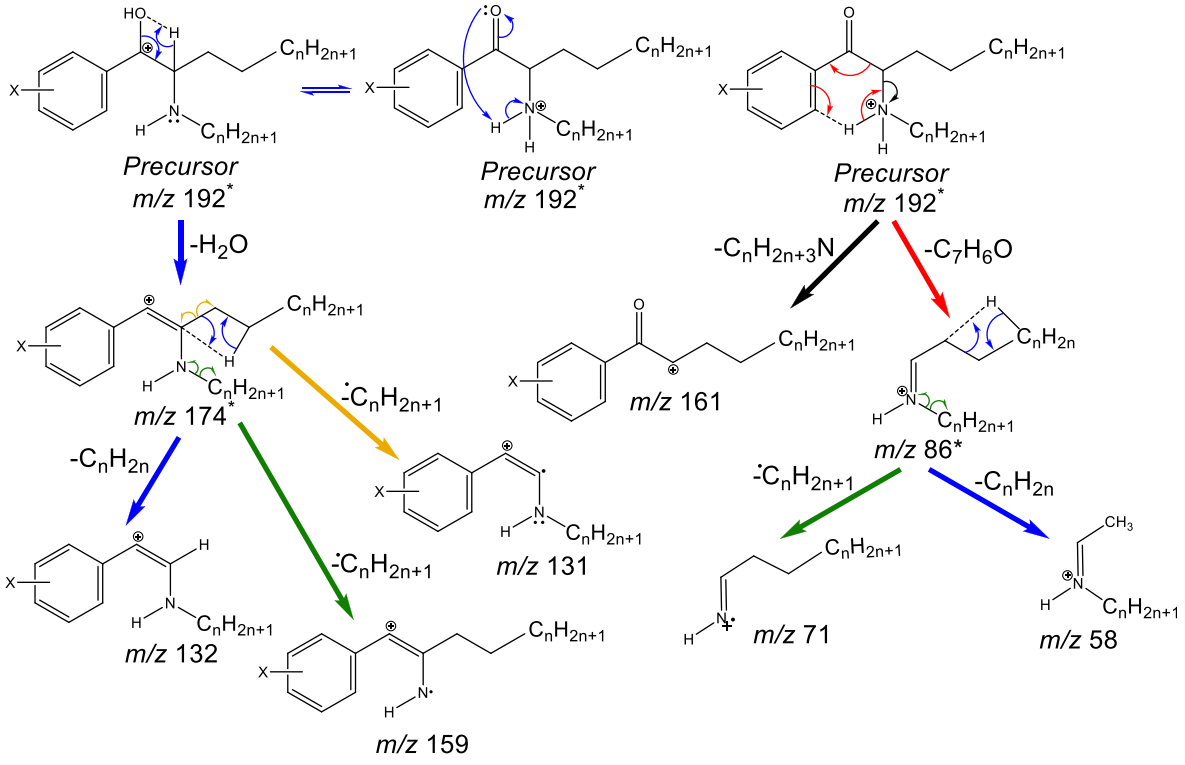

Fig. 7. Proposed mechanisms for fragmentation pathways of *N*-alkylated synthetic cathinones. The model compound is pentedrone (aliphatic group = CH_3, *N*-alkyl group = CH_3, X = H) with ions specific to pentedrone indicated with an asterisk (*); different functional groups, X, will shift the product ion *m/z* values accordingly. The most stable resonant form is not always shown.

N-alkylated synthetic cathinones is the formation of the valerophenone-like ion at *m/z* 161 through the loss of $C_nH_{2n+3}N$ (black pathway in Fig. 7). The secondary and tertiary product ions deriving from the valerophenone-like intermediate have been described extensively for α-pyrrolidinophenone synthetic cathinones [26]. They include fragments at *m/z* 133 and *m/z* 119, which have a phthalane-like structure, and the tropylium ion at *m/z* 91 [17].

Similar to the α-pyrrolidinophenones studied previously [26], which have a facile leaving group in the form of pyrrolidine, fragmentation via the loss of a neutral 3° amine was the dominant fragmentation pathway for the 3° amines analyzed here. The other observed fragmentation pathway for 2° and 3° amines is through the loss of C_7H_6O (red pathway) to form iminium ions similar to the one at *m/z* 86 for pentedrone in Fig. 7. This pathway is readily explained via a McLafferty rearrangement and leads to secondary fragments through the loss of alkyl radicals from the *N*-alkyl chain (green pathway) and even-electron alkenes through 4- or 6-center eliminations from the aliphatic chain (blue pathway).

3.3. GC-EI-MS

The previous literature on the analysis of phenethylamines with GC-EI-MS has documented the need to identify phenethylamines, their metabolites and their thermal degradation products, the latter of which can occur in the injection port or on-column and are often observed as a shoulder or split peak in the GC [5,31,32]. The 2,3-enamine degradation products observed from the *N*-alkylated synthetic cathinones in this project were always minor relative to the abundance of the precursor compound. Fig. 8 shows the GC-EI-MS spectrum of ^{13}C-ethylone, which is isotopically labeled with ^{13}C on the carbonyl carbon. The extensive fragmentation caused by EI occurs through well-established fragmentation mechanisms such as the formation of the benzoylium ion at *m/z* 105 or iminium ion ($C_nH_{2n+2}N^+$) at *m/z* 72 for ethylone [28]. The established fragmentation mechanisms for EI-MS are both radical-directed and charge-directed, in contrast to the charge-remote, 4- and 6-center eliminations commonly observed in protonated tandem mass spectra. The iminium ions are so dominant in EI that competing fragmentation pathways are of low abundance (<10% base peak) and provide minimally informative spectra [33]. Fig. 8 contains the embedded major structural fragments. The spectrum has been truncated to *m/z* 40–200 because the molecular ion at *m/z* 222 was not observed. The most abundant structural fragments are the methylenedioxy-substituted benzoylium and phenylium ions at *m/z* 150 and 121, respectively, and the iminium ion observed at *m/z* 72. Note that the low-abundance methylenedioxy-substituted tropylium ion at *m/z* 135 is 14 Da heavier than the structure shown at *m/z* 121 and therefore requires extensive rearrangements after the initial loss of an alkane radical [17].

The GC-EI-MS spectrum of α-propylaminopentiophenone (Fig. 9) follows the same fragmentation behavior as ^{13}C-ethylone, with the formation of the iminium, benzoylium and phenylium ions of significant abundance. The molecular ion at *m/z* 219 is not observed, and the fragmentation pattern is consistent with previous work [29]. However, α-propylaminopentiophenone has a propyl amine and pentyl aliphatic chain, leading to the formation of the iminium ion at *m/z* 114 in Fig. 9. The iminium ion can fragment further to form another iminium ion at *m/z* 72 through the loss of a propene neutral.

Fig. 10 shows the GC-EI-MS spectrum of ^{13}C-benzedrone—isotopically labeled on the carbonyl carbon—with the major structural fragments embedded. This compound is unique in that the *N*-alkylated moiety contains an aromatic ring. The aromatic

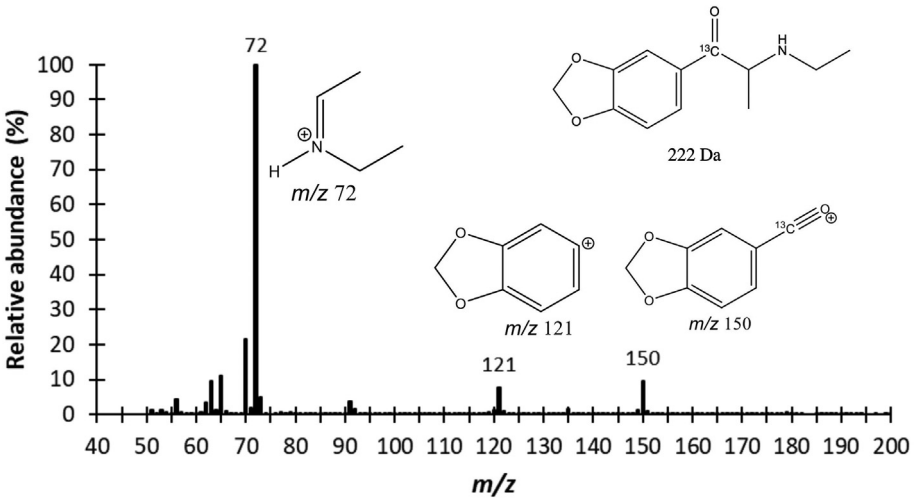

Fig. 8. Full scan mass spectra of ^{13}C-ethylone (isotopically labeled with ^{13}C on the carbonyl carbon) collected with GC-EI-MS.

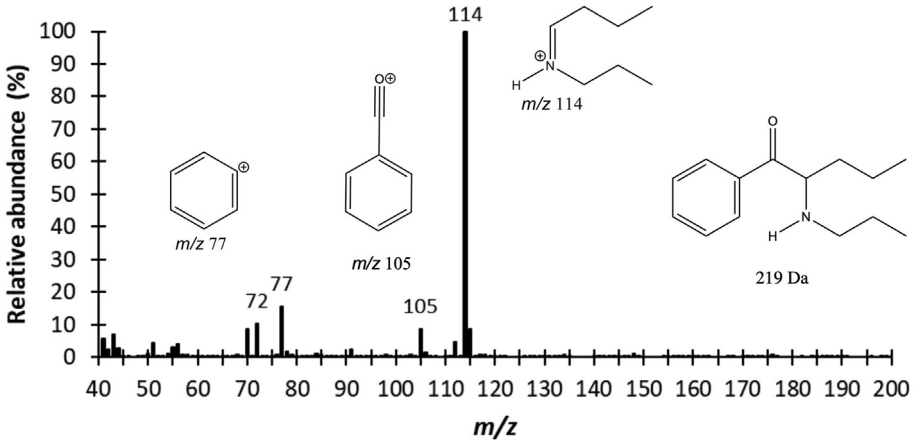

Fig. 9. Full scan mass spectra of α-propylaminopentiophenone collected with GC-EI-MS.

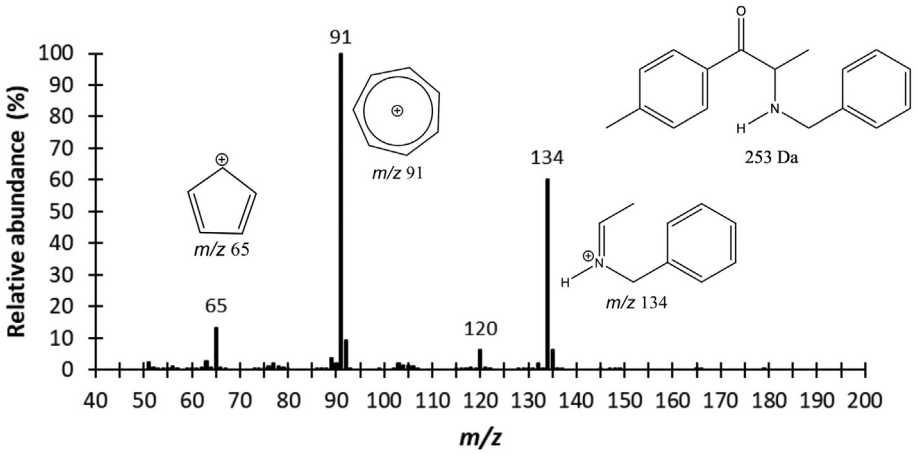

Fig. 10. Full scan mass spectra of ^{13}C-benzedrone collected with GC-EI-MS.

ring causes a notable shift in the fragmentation behavior of this compound. For example, the base peak of Fig. 10 is the tropylium ion at *m/z* 91, which forms through charge-directed cleavage of the aromatic moiety. The aromatic substituted iminium ion (*m/z* 134), ^{13}C-labeled methyl substituted phenylethyl ion (*m/z* 120), and cyclopentadienyl ion (*m/z* 65) are structural ions of significant abundance.

Three additional GC-EI-MS figures are included in the

supplemental material as representative examples for other compounds analyzed in this study. Fig. 11 contains the proposed EI-MS fragmentation mechanisms for the *N*-alkylated class of synthetic cathinones, where X represents substitution to the phenyl moiety and C_nH_{2n+1} represents varying alkyl chain lengths. Pentedrone is the model compound for illustrative purposes. The isotopic labels are not shown in Fig. 11 but were used to further support the proposed mechanisms. The acylium (red pathway) and iminium ions (blue pathway) are the dominant fragmentation behavior for *N*-alkylated synthetic cathinones. The acylium ion pathway is initiated by α-cleavage of the bond between the carbonyl carbon and the α-carbon adjacent to the amine. The subsequent loss of CO from the acylium ion produces the phenylium ion at *m/z* 77, which can then ring-contract to lose C_2H_2 to form the cyclobutadienyl cation at *m/z* 51. The iminium ion cascade is initiated by a radical electron on the nitrogen and α-cleavage of the bond between the carbonyl carbon and the α-carbon adjacent to the pyrrolidine ring.The iminium ion pathway can form secondary fragments through 4- or 6-center eliminations along the alkyl chain (black pathway) and radical-directed cleavage (gold pathway). The benzoylium ion can also form through α-cleavage of the bond between the carbonyl carbon and the α-carbon, which is initiated or stabilized by a lone pair of electrons on the oxygen atom (green pathway).

4. Conclusions

The combination of isotopic labeling, MS^n, and HRMS was used to further develop our current understanding of the fragmentation behavior of the *N*-alkylated class of synthetic cathinone derivatives. In addition, a comparison between three different ionization and fragmentation techniques commonly available in crime laboratories provides insight into the fragmentation behavior of these compounds under different instrumental conditions. The most common mass spectrometer used for seized drug analysis is GC-EI-MS, whereas the toxicological community typically employs LC-ESI-MS/MS and more recently the community has increased the use of ambient ionization, such as DART. The identification of characteristic fragmentation pathways provides practitioners with an additional tool for the identification of *N*-alkylated synthetic cathinones.

The protonated tandem mass spectrometry fragmentation pathways and proposed fragmentation mechanisms were developed based on the analysis of a series of *N*-alkylated synthetic cathinone derivatives. The LIT instrument provided the capability to identify the direct relationship between each ion along the proposed fragmentation pathways using MS^n analysis. In comparison, the Q-TOF mass spectrometer identified the elemental formulas by comparing the accurate mass measurements with the theoretical exact mass measurements. The identification of fragmentation pathways that are conserved between ion trap- and beam-type mass spectrometers provides additional confidence, although the multi-collisional environment of the ion trap tends to favor low-energy pathways and higher-mass ions [22]. Finally, both ESI and DART ion sources produced intact protonated molecular ions with very similar protonated tandem mass spectra for all the

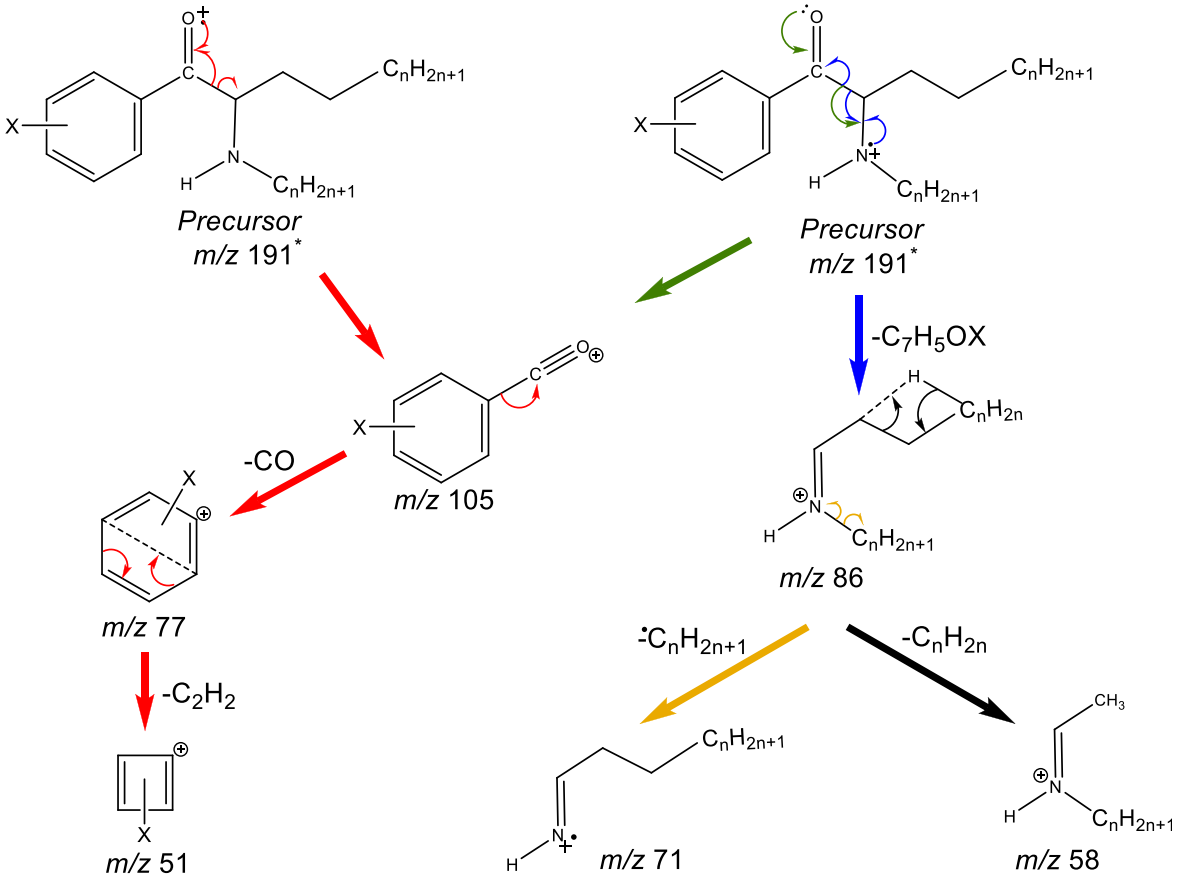

Fig. 11. Proposed EI-MS fragmentation mechanisms for the *N*-alkylated class of synthetic cathinones (adapted from Ref. [26,34]). The model compound is pentedrone (aliphatic group = CH_3, *N*-alkyl group = CH_3, X = H) with ions specific to pentedrone indicated with an asterisk (*).

analogs studied.

The diagnostic ions formed with protonated tandem mass spectrometry occur through the loss of H_2O, $C_nH_{2n+3}N$, and C_7H_6O, as displayed in Fig. 7. The loss of H_2O appears to be the dominant pathway for 2° amines, which is in stark contrast to 3° amines, which favor the formation of alkylphenones via the loss of imine neutrals. The hydrogens lost as H_2O do not originate from the *N*-alkyl groups or the terminal carbon of the alkyl chains, but instead originate from the protonating hydrogen and an H atom nearer the carbonyl group. The formation of characteristic secondary fragmentation for 2° amines occurs through the loss of alkenes (C_nH_{2n}) from the amine moiety and alkyl radicals ($\dot{C}_nH_{2n+1}$) from both the amine and aliphatic chains. The same fragmentation behavior is observed for the iminium ion fragmentation pathway through the loss of alkyl radicals ($\dot{C}_nH_{2n+1}$) and alkenes (C_nH_{2n}) from the amine moiety.

In contrast to CID of protonated precursors, EI-MS spectra of *N*-alkylated synthetic cathinones are dominated by radical-directed cleavages that lead to acylium and iminium ions. One down-side to the conserved iminium ions is when one observes, say, a 42-Da shift in the iminium ion from ethylone to α-propylaminopentiophenone one cannot readily confirm whether the three additional methylene groups are on the aliphatic chain, the *N*-alkyl chain or a combination of the two.

The proposed fragmentation mechanisms for the protonated tandem mass spectrometry and EI-MS pathways provide rational explanations for the observed fragmentation behavior based on the combination of isotopic labeling, MS^n, HRMS, and EI-MS. The significance of identifying fragmentation mechanisms is the application of this knowledge to novel compound identification. The interrogation of collected mass spectra against the proposed fragmentation pathways provides an additional tool for the identification of novel *N*-alkylated synthetic cathinones. Finally, providing fragmentation pathways and mechanistic explanations that are applicable across a range of ionization and fragmentation conditions provides useful multi-discipline mass spectral interpretation to practitioners.

Funding

This project was supported by grant number 2018-75-CX-0033, awarded by the National Institute of Justice, Office of Justice Programs, and U.S. Department of Justice. The opinions, findings, and conclusions or recommendations expressed in this publication are those of the authors and do not necessarily reflect the views of the Department of Justice.

Declaration of competing interest

The authors declare that they have no known competing financial interests or personal relationships that could have appeared to influence the work reported in this paper.

CRediT authorship contribution statement

J. Tyler Davidson: Conceptualization, Methodology, Formal analysis, Writing - original draft. **Zachary J. Sasiene:** Formal analysis, Writing - review & editing. **Glen P. Jackson:** Conceptualization, Project administration, Methodology, Writing - review & editing.

Acknowledgements

This project was supported by grant number 2018-75-CX-0033, awarded by the National Institute of Justice, Office of Justice Programs, U.S. Department of Justice. The opinions, findings, and conclusions or recommendations expressed in this publication are those of the authors and do not necessarily reflect the views of the Department of Justice.

Appendix A. Supplementary data

Supplementary data to this article can be found online at https://doi.org/10.1016/j.ijms.2020.116354.

References

[1] M.J. Valente, P. Guedes de Pinho, M. de Lourdes Bastos, F. Carvalho, M. Carvalho, Khat and synthetic cathinones: a review, Arch. Toxicol. 88 (1) (2014) 15–45, https://doi.org/10.1007/s00204-013-1163-9.
[2] A.D. Krikorian, Khat and its use: an historical perspective, J. Ethnopharmacol. 12 (2) (1984) 115–178.
[3] J.P. Kelly, Cathinone derivatives: a review of their chemistry, pharmacology and toxicology, Drug Test. Anal. 3 (2011) 439–453, https://doi.org/10.1002/dta.313.
[4] L.L. Ioannides-Demos, L. Piccenna, J.J. McNeil, Pharmacotherapies for obesity: past, current, and future therapies, J. Obes. 2011 (2011) 1–18, https://doi.org/10.1155/2011/179674.
[5] J. DeRuiter, L. Hays, A. Valaer, C.R. Clark, Methcathinone and designer drug analogs: synthesis, stereochemical analysis, and analytical properties, J. Chromatogr. Sci. 32 (1994) 552–564.
[6] M.G. Bossong, J.P. Van Dijk, R.J. Niesink, Methylone and mCPP, two new drugs of abuse?, Addict, Biol. 10 (4) (2005) 321–323, https://doi.org/10.1080/13556210500350794.
[7] A.L. Bretteville-Jensen, S.S. Tuv, O.R. Bilgrei, B. Field, L. Bachs, Synthetic cannabinoids and cathinones: prevalence and markets, Forensic Sci. Rev. 25 (2013) 7–26.
[8] K. Zaitsu, M. Katagi, M. Tatsuno, T. Sato, H. Tsuchihashi, K. Suzuki, Recently abused β-keto derivatives of 3,4-methylenedioxyphenylalkylamines: a review of their metabolisms and toxicological analysis, Forensic Toxicol. 29 (2) (2011) 73–84, https://doi.org/10.1007/s11419-011-0111-8.
[9] K.N. Ellefsen, M. Concheiro, M.A. Huestis, Synthetic cathinone pharmacokinetics, analytical methods, and toxicological findings from human performance and postmortem cases, Drug Metab. Rev. 48 (2) (2016) 237–265, https://doi.org/10.1080/03602532.2016.1188937.
[10] B.L. Murray, C.M. Murphy, M.C. Beuhler, Death following recreational use of designer drug "bath salts" containing 3,4-Methylenedioxypyrovalerone (MDPV), J. Med. Toxicol. 8 (1) (2012) 69–75, https://doi.org/10.1007/s13181-011-0196-9.
[11] Schedules of controlled substances; placement of methcathinone into schedule I, fed, Regist 58 (198) (1993) 53404–53406.
[12] M. Majchrzak, R. Celinski, P. Kus, T. Kowalska, M. Sajewicz, The newest cathinone derivatives as designer drugs: an analytical and toxicological review, Forensic Toxicol. 36 (1) (2018) 33–50, https://doi.org/10.1007/s11419-017-0385-6.
[13] E. Fornal, Study of collision-induced dissociation of electrospray-generated protonated cathinones, Drug Test. Anal. 6 (2014) 705–715, https://doi.org/10.1002/dta.1573.
[14] L. Bijlsma, J.V. Sancho, F. Hernandez, W.M. Niessen, Fragmentation pathways of drugs of abuse and their metabolites based on QTOF MS/MS and MS(E) accurate-mass spectra, J. Mass Spectrom. 46 (9) (2011) 865–875, https://doi.org/10.1002/jms.1963.
[15] J.D. Power, S.D. McDermott, B. Talbot, J.E. O'Brien, P. Kavanagh, The analysis of amphetamine-like cathinone derivatives using positive electrospray ionization with in-source collision-induced dissociation, Rapid Commun. Mass Spectrom. 26 (22) (2012) 2601–2611, https://doi.org/10.1002/rcm.6383.
[16] A. Namera, M. Kawamura, A. Nakamoto, T. Saito, M. Nagao, Comprehensive review of the detection methods for synthetic cannabinoids and cathinones, Forensic Toxicol. 33 (2) (2015) 175–194, https://doi.org/10.1007/s11419-015-0270-0.
[17] J.T. Davidson, E.L. Piacentino, Z.J. Sasiene, Y. Abiedalla, J. DeRuiter, C.R. Clark, G. Berden, J. Oomens, V. Ryzhov, G.P. Jackson, Identification of novel fragmentation pathways and fragment ion structures in the tandem mass spectra of protonated synthetic cathinones, Forens. Chem 19 (2020), https://doi.org/10.1016/j.forc.2020.100245.
[18] O.J. Pozo, M. Ibanez, J.V. Sancho, J. Lahoz-Beneytez, M. Farre, E. Papaseit, R. de la Torre, F. Hernandez, Mass spectrometric evaluation of mephedrone in vivo human metabolism: identification of phase I and phase II metabolites, including a novel succinyl conjugate, Drug Metab. Dispos. 43 (2) (2015) 248–257, https://doi.org/10.1124/dmd.114.061416.
[19] P. Jankovics, A. Varadi, L. Tolgyesi, S. Lohner, J. Nemeth-Palotas, H. Koszegi-Szalai, Identification and characterization of the new designer drug 4'-methylethcathinone (4-MEC) and elaboration of a novel liquid chromatography-tandem mass spectrometry (LC-MS/MS) screening method for seven different methcathinone analogs, Forensic Sci. Int. 210 (2011) 213–220, https://doi.org/10.1016/j.forsciint.2011.03.019.

[20] J. Martinez-Clemente, R. Lopez-Arnau, M. Carbo, D. Pubill, J. Camarasa, E. Escubedo, Mephedrone pharmacokinetics after intravenous and oral administration in rats: relation to pharmacodynamics, Psychopharmacology 229 (2) (2013) 295–306, https://doi.org/10.1007/s00213-013-3108-7.
[21] E. Fornal, Identification of substituted cathinones: 3,4-Methylenedioxy derivatives by high performance liquid chromatography-quadrupole time of flight mass spectrometry, J. Pharmaceut. Biomed. Anal. 81–82 (2013) 13–19, https://doi.org/10.1016/j.jpba.2013.03.016.
[22] L. Sleno, D. Volmer, Ion activation methods for tandem mass spectrometry, J. Mass Spectrom. 39 (2004) 1091–1112.
[23] F.W. McLafferty, Mass spectrometric analysis molecular rearrangements, Anal. Chem. 31 (1) (1959) 82–87.
[24] M. Cydzik, M. Rudowska, P. Stefanowicz, Z. Szewczuk, The competition of charge remote and charge directed fragmentation mechanisms in quaternary ammonium salt derivatized peptides–an isotopic exchange study, J. Am. Soc. Mass Spectrom. 22 (12) (2011) 2103–2107, https://doi.org/10.1007/s13361-011-0245-2.
[25] E. Fornal, Formation of odd-electron product ions in collision-induced fragmentation of electrospray-generated protonated cathinone derivatives: aryl alpha-primary amino ketones, Rapid Commun. Mass Spectrom. 27 (16) (2013) 1858–1866, https://doi.org/10.1002/rcm.6635.
[26] J.T. Davidson, Z.J. Sasiene, Y. Abiedalla, J. DeRuiter, C.R. Clark, G.P. Jackson, Fragmentation pathways of α-pyrrolidinophenone derivative synthetic cathinones and their application to the identification of novel synthetic cathinone derivatives, Int. J. Mass Spectrom. (2020), https://doi.org/10.1016/j.ijms.2020.116343. In Press.
[27] R.B. Cody, Why are we still reporting mass accuracy in parts per million (ppm)? J. Am. Soc. Mass Spectrom. 31 (4) (2020) 1004–1005, https://doi.org/10.1021/jasms.9b00150.
[28] D. Zuba, Identification of cathinones and other active components of 'legal highs' by mass spectrometric methods, Trends Anal. Chem. 32 (2012) 15–30, https://doi.org/10.1016/j.trac.2011.09.009.
[29] M. Majchrzak, R. Celinski, T. Kowalska, M. Sajewicz, Fatal case of poisoning with a new cathinone derivative: alpha-propylaminopentiophenone (N-PP), Forensic Toxicol. 36 (2) (2018) 525–533, https://doi.org/10.1007/s11419-018-0417-x.
[30] Wilfried M.A. Niessen, R.A. Correa, Interpretation of MS-MS Mass Spectra of Drugs and Pesticides: Chapter 4 Fragmentation of Drugs and Pesticides, John Wiley & Sons, 2017, pp. 241–247.
[31] A.H. Beckett, G.R. Jones, D.A. Hollingsbee, Degradation of (-)-ephedrine in solution and during extraction with diethyl ether, J. Pharm. Pharmac. 30 (1978) 15–19.
[32] S. Kerrigan, M. Savage, C. Cavazos, P. Bella, Thermal degradation of synthetic cathinones: implications for forensic toxicology, J. Anal. Toxicol. 40 (1) (2016) 1–11, https://doi.org/10.1093/jat/bkv099.
[33] M.P. Levitas, E. Andrews, I. Lurie, I. Marginean, Discrimination of synthetic cathinones by GC-MS and GC-MS/MS using cold electron ionization, Forensic Sci. Int. 288 (2018) 107–114, https://doi.org/10.1016/j.forsciint.2018.04.026.
[34] S. Matsuta, M. Katagi, H. Nishioka, H. Kamata, K. Sasaki, N. Shima, T. Kamata, A. Miki, M. Tatsuno, K. Zaitsu, K. Tsuboi, H. Tsuchihashi, K. Suzuki, Structural characterization of cathinone-type designer drugs by EI mass spectrometry, Jpn. J. Forensic Sci. Technol. 19 (2) (2014) 77–89.